

# Multitemporal Monitoring of Land Degradation Risk Due to Soil Loss in a Fire-Prone Mediterranean Landscape Using Multi-decadal Landsat Imagery

Giorgos Mallinis<sup>1</sup>  · Ioannis Z. Gitas<sup>2</sup> ·  
Georgios Tasionas<sup>1</sup> · Fotis Maris<sup>3</sup>

Received: 13 February 2015 / Accepted: 4 January 2016 /  
Published online: 16 January 2016  
© Springer Science+Business Media Dordrecht 2016

**Abstract** Natural, as well as human-induced, landscape changes may have profound effects on soil-loss rates in Mediterranean countries. Knowledge of the spatial and temporal distribution of the erosion processes from 1984 to 2013 across the fire-prone island of Thassos was gained on the basis of a joint analysis of imagery received from three generations of Landsat

---

## Highlights

- This study presents spatial and temporal changes of soil loss in a Mediterranean fire prone landscape and its linkages with wildfire impacts and human-induced disturbances.
- Due to their subtle differences, vegetation indices derived from different Landsat satellites were used complementary for the temporal study of the phenomenon. following correction of atmospheric and cross-sensor inconsistencies.
- The soil loss is more evident in south facing slopes and steep gradients similar to the findings of plot-scale studies in Mediterranean areas.

---

✉ Giorgos Mallinis  
gmallin@fmenr.duth.gr

Ioannis Z. Gitas  
igitas@for.auth.gr

Georgios Tasionas  
giw\_tasi@hotmail.com

Fotis Maris  
fmaris@fmenr.duth.gr

<sup>1</sup> Laboratory of Forest Remote Sensing, Department of Forestry and Management of the Environment and Natural Resources, Democritus University of Thrace, Orestiada, Greece

<sup>2</sup> Laboratory of Forest Management and Remote Sensing, Department of Forestry and Natural Environment, Aristotle University of Thessaloniki, Thessaloniki, Greece

<sup>3</sup> Laboratory of Mountainous Watersheds and Risk Management, Department of Forestry and Management of the Environment and Natural Resources, Democritus University of Thrace, Orestiada, Greece

satellites. Soil loss was modeled using the revised universal soil loss equation. With the exception of the crop management factor, which was estimated through the NDVI image series, rainfall erosivity, soil erodibility, and topographic factor, were compiled within a GIS environment and used for the production of the spatio-temporal erosion maps. We found some constant patterns regarding the spatial distribution of soil susceptibility to erosion, similar to the findings of plot scale studies in the Mediterranean, as well as major changes related to the temporal intensity of the process. With regard to the aspect, we found that the most erosion-prone areas diachronically were the south-facing slopes. The highest altitudinal zone was most at soil-loss risk, but this elevation zone occupies the smallest spatial extent compared to the others. We observed a major increase for all the elevation and aspect zones, as well for every watershed of the island, during 1984–1991, when Thassos experienced some catastrophic fires. Between 1984 and 2013, all but one the watersheds of the island experienced a severe increase in soil erosion, suggesting the need for prevention measures and restoration plans that specifically target the areas most vulnerable to degradation. Quantification of the soil loss over large areas and large time extents, can contribute to an understanding of the process, highlight drivers of change and assist in the implementation of erosion control measures and decision making.

**Keyword** RUSLE · NDVI · Fire · Soil erosion · GIS

## 1 Introduction

Although it is a natural process inherent in landscape evolution throughout history, soil erosion is also a major worldwide environmental and agricultural problem that has greatly intensified in recent years (Morgan 2005). In Mediterranean countries particularly, soil erosion is a prominent cause of land degradation and desertification (Cerdà et al. 2010), due to adverse climate, step terrain, natural disasters, and natural and human landscape modifications (Mallinis et al. 2009). Especially, Land Use/land Cover Changes (LUCC) due to wildfires can be perceived as the major, direct and direct cause of change on hydrological and geomorphological processes, in fire-prone Mediterranean landscapes (Shakesby and Doerr 2006).

Soil erosion and land degradation resulting from LUCC have attracted the attention of numerous researchers (Bajocco et al. 2011; Siyuan et al. 2007; Zhao et al. 2012). Knowledge of the spatial and temporal distribution of the erosion processes at different scales, is crucial for sustainable resources management plans and spatial explicit conservation measures in order to mitigate land degradation.

Diachronic continuous soil loss monitoring based on field measurements while the most accurate approach for understanding soil loss and erosion dynamics over these dynamic landscapes (Wittenberg and Inbar 2009), it is very expensive, and time consuming, and spatially impractical over landscape scales (Liu et al. 2015). Therefore there is a relatively poor understanding of the magnitude of change and drivers of soil loss at scales larger than small plots since most erosion monitoring studies have been carried out at small spatial scales (transects, small plots and, rarely, hillslope measurements) and short temporal scales with relatively few studies carried out at larger scales (Shakesby and Doerr 2006). Multitemporal mathematical modelling of soil loss at landscape scales, can be used in order to understand the degradation processes and effects at both larger spatial and temporal scales.

With regard to spatial explicit soil erosion and sediment yield prediction at landscape scales, different models and relationships have been proposed, with many of these having a high data demand, thus limiting their applicability in data-rich environments, or after extensive collection of field data on model parameters (Merritt et al. 2003). The Universal Soil Loss Equation (USLE) model (Wischmeier and Smith 1978), and its improved version (Revised USLE or RUSLE) (Renard et al. 1997) are among the models most commonly used to predict the mass of eroded soil in various domains such as post-fire effects mitigation (Miller et al. 2003), management of sediment deposits on roadways (Morschel et al. 2004), watershed prioritization (Jaiswal et al. 2015), sedimentation in water reservoirs (Butt et al. 2010), land management decision-making (Tamene et al. 2014) and country-level soil loss assessments (Chou 2010).

The framework for efficiently implementing such models that allows accurate and robust modelling and analysis of soil erosion and land degradation (Vrieling 2006) is provided within Geographic Information Systems (GIS) environment along with satellite remote sensing and spatially explicit ancillary data. To this end, Landsat imagery, providing the longest continuous space-based record of Earth's land in existence, with its unique combination of spatial, spectral, and temporal resolution and extent, has been the primary source of medium spatial resolution earth observations that have been used for quantifying the effect of landscape composition and LUCC in the soil loss and land degradation process in Mediterranean areas and elsewhere (Kumar and Mishra 2015; Lu et al. 2007; Mallinis et al. 2009; Wang et al. 2013).

The main goal of our study is to monitor and assess soil loss and its spatiotemporal changes in the fire prone Mediterranean island of Thassos during the 1984–2013 period using imagery coming from Landsat TM, ETM+ and OLI sensors.

The specific objectives of this study included (1) generation of NDVI images that are used to infer the spatial distribution of vegetation cover, while considering the impact of cross-sensor inconsistencies (2) quantification of soil loss and land degradation over Thassos over 5 different time points between 1984 and 2013 (3) assess the differences in soil loss process observed in the context of historical wildfire regime and other human induced changes occurring in the island during the last 3 decades.

## 2 Study Area

Thassos is the most northerly island in the Aegean Sea, prefecture of Kavala, extending from 24°30' to 24°48' East, and 40°33' to 40°49' North (Fig. 1). Its surface area is 380 sq.km. The island is mountainous with intense relief. Elevation ranges from sea level to 1203 m and the terrain slopes range from 0° to 76°. The climate of Thassos is cool and humid Mediterranean, with mean annual precipitation and temperature being 691 mm and 15.9 °C, respectively (Kaltsas et al. 2007). The island belongs to the Mediterranean vegetation eco-zone characterized by thermophile broad-leaved evergreen shrubs, and pure stand forests of *Pinus brutia* and *Pinus nigra* (Gitas and Devereux 2006). In addition to forested vegetation, other types of sclerophyllous Mediterranean vegetation are also found, such as maquis and garrigue (Mouflis et al. 2008). The rural sector is traditionally devoted to the cultivation of olive trees, and olive groves dominate many landscapes of the island.

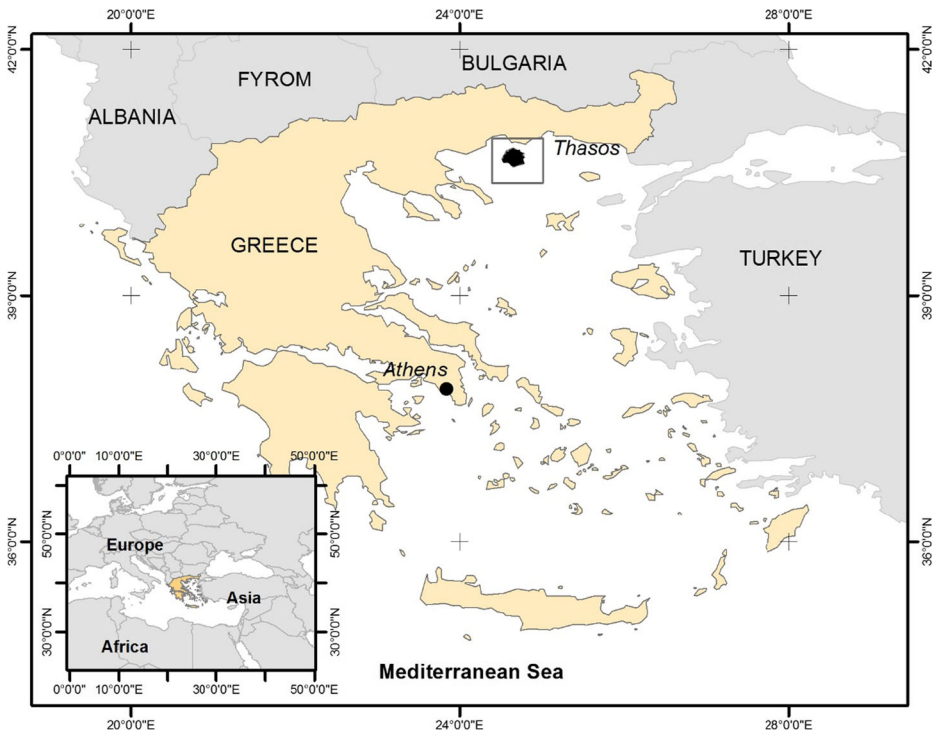


**Fig. 1** Study area

### 3 Materials and Methods

#### 3.1 Satellite Data and Pre-processing

With regard to remote sensing data, satellite images (path/row 183/032 and 182/032) received from Landsat-4 and Landsat-5 Thematic Mapper (TM), Landsat-7 Enhanced Thematic Mapper (ETM+) and Landsat-8 Operational Land Imager (OLI) sensors were used to monitor the vegetative cover of Thassos in 1984, 1991, 2000, 2007, and 2013. Compared to its predecessors, the Landsat-8 OLI sensor has a greater number of bands and narrower spectral ranges; however, it maintains 30 m spatial resolution, as well as 16-day temporal resolution and scene size (170 km × 183 km) with push-broom design.

Image acquisition days were selected during the July–September period, in order to capture similar phenological states of the vegetation. For each of the 1984 and 1991 time points, one additional image was used in order to compensate for information gaps due to cloud cover.

Images employed in the analysis are processed to Standard Terrain Correction (Level 1 T), which provides systematic radiometric and geometric accuracy by incorporating ground control points while employing a DEM for topographic accuracy. Visual assessment indicated the lack of any mis-registration errors; therefore, all images were re-projected to the Hellenic Geodetic Reference System 1987.

In the next step, radiometric corrections were applied to the Landsat image sequence, in order to minimize errors and noise related to changes in illumination, atmospheric conditions and viewing geometry. To ensure consistency in the multi-temporal assessment and

comparison of land degradation due to soil loss, digital number (DN) values were transformed to surface reflectance and the dark object subtraction approach was applied to correct the effects caused by the solar zenith angle, solar radiance, and atmospheric scattering. One advantage of this image-based approach is that it is relatively simple to apply and does not require any in situ measurements and atmospheric parameters (Chavez 1996).

### 3.2 Ancillary Data

High resolution digital elevation model (DEM) data are required for the computation of topographic factor, as is general in spatially distributed hydrologic modeling over complex terrain (Miller et al. 2003). Therefore a 10-m DEM of Thassos was created through digitization of 4 m contour lines from 1:5000 topographic maps in order to generate the topographic (LS) factor. All subsequent modeling was performed at 10 m resolution. An analog soil sheet map using a 1:50000 scale was digitized in order to include relevant information on the analysis process (Nakos 1979). The vector outlines of Thassos watersheds were obtained from the Greek Ministry of Environment, Energy & Climate Change. Finally, the geo-database of recent fire history of the island was compiled based on fire scars extracted on an annual basis from available Landsat imagery acquired in late autumn, designating the end of the fire season.

### 3.3 Soil Loss Modeling

The USLE is one of the most widely used erosion prediction models (Wischmeier and Smith 1978) as is the updated version, the RUSLE (Renard et al. 1997). The RUSLE computes erosion as a linear combination of factors:

$$A = R \times K \times LS \times C \times P \quad (1)$$

where A is the computed spatial and temporal average soil loss per unit area, expressed in the units selected for K and for the period selected for R; R is the rainfall/runoff erosivity factor; K is the soil erodibility factor; LS or 'topographic factor' is the combined effect of slope length (L) and slope steepness factor (S); C is the cover-management factor; and P is the support practice factor.

#### 3.3.1 Land Cover Management (C) Factor

A common method used for spatial explicit representation of C factor is the assignment of values to various LULC classes by means of a lookup-table, using existing thematic maps or classified remotely sensed images of study areas (Kumar et al. 2014). However, this approach contains some inherent limitations related to either the difficulty in identifying reliable training samples, in the case of supervised approaches, or in specifying the appropriate number of clusters or groups when following unsupervised procedures, as well as limitations related to the uncertainty of the error magnitude present in historical images classification, due to the lack of validation datasets.

An alternative approach for estimating the spatial distribution of the C-factor is the use of satellite-based vegetation indices, which are quantitative measures related to vegetation spectral properties and express biomass or vegetative vigor. The most widely used remote-sensing

derived indicator of vegetation growth is the NDVI (Tucker 1979), which is estimated by the following computing formula:

$$NDVI = \frac{NIR - Red}{NIR + Red} \quad (2)$$

where NIR and Red is the reflectance recorded in near-infrared and red spectrum, respectively.

On the basis of the NDVI image, the following equation, which gives better results than assuming a linear relationship, is used to generate a C- factor surface from NDVI values (Van der Knijff et al. 1999):

$$C = \exp \left[ -a \left( \frac{NDVI}{b - NDVI} \right) \right] \quad (3)$$

where  $\alpha$  equals 2 and  $\beta$  equals 1, which are unit less parameters that determine the shape of the curve relating to NDVI and the C-factor.

While NDVI, as well as other broadband vegetation indices, exhibits low sensitivity to the uncertainties in atmospheric conditions and the variation in the satellite viewing angle, when indices from different monitoring systems are combined, or used jointly in a long time series, inconsistencies in the data may be found, due to cross-sensor radiometry, (e.g., bandwidth and spectral band pass filter responses, seasonal temperature-related phenology) (Simms and Ward 2013; Steven et al. 2003). Therefore, a relative calibration procedure normalization, which involves image bands radiometric matching in a time-series to an atmospherically corrected reference image using pseudo-invariant features (PIFs) was adopted for the red and near-infrared bands of the images (Schroeder et al. 2006). This procedure assumes that the pixels sampled at the image to be adjusted are linearly related to the pixels, of the same locations, sampled at the reference image, and that the spectral reflectance properties of the sampled pixels are consistent during the time interval (Paolini et al. 2006).

The calibration was based on regression equations obtained from 67 points, each chosen to represent PIFs throughout the island. The bright (quarries), medium (sparsely vegetated areas), and dark (dense forests) features were selected to encompass the full range of spectral brightness found across the island.

### 3.3.2 Rainfall Erosivity (R)

The R factor for any given period is obtained as the average annual sum of the kinetic energy products of each storm with, maximum, 30-min rainfall intensity (Renard et al. 1997). Since pluviograph and detailed rainstorm data are rarely available at standard meteorological stations, mean annual and monthly rainfall amounts have often been used to estimate the R factor for the RUSLE (Kouli et al. 2009). To calculate the R-factor, Eq. (2), was used because the R-factor equation of Renard et al. (1997) requires rainfall intensity data, which were not available inside the study area.

According to this equation, the R factor is estimated using the mean annual rainfall (P), according to the formula recommended for Thassos by Flabouris (2008):

$$R = P \times a \quad (4)$$

where  $a$  is equal to 0.7 for the study area.

For each site, a constant rainfall erosivity factor (R) and the input data layers for mean monthly rainfall were created using a preprocessing step that projected gridded data for mean

monthly precipitation from the WorldClim project (Hijmans et al. 2005). The spatial distribution map of the R factor was produced by applying Eq. (8) to the mean annual rainfall data.

### 3.3.3 Soil Erodibility (K) Factor

The soil erodibility factor (K) reflects the characteristics of the soil and represents its inherent susceptibility to detachment and transport by rainfall and runoff (Kumar et al. 2014). The K factor is rated on a scale from 0 to 1, with 0 indicating soils with the least susceptibility to erosion, and 1 indicating soils that are highly susceptible to soil erosion.

The K factor values assigned to the geological formations are presented in Table 1, and were based on inference with expertise (Karydas et al. 2013). The corresponding map was generated by reclassifying the soil map.

### 3.3.4 Topographic LS Factor

The combined topographic (LS) factor is a function of both slope steepness factor (S) and slope length factor (L) and is considered to be a crucial factor in the quantification of erosion due to surface run-off (Renard et al. 1997). The slope length (L) is defined as the distance from the origin of overland flow to the point where deposition begins to occur (Renard et al. 1997) while slope steepness (S) refers to the effect of the slope gradient on erosion in comparison to the standard plot steepness of 9 %.

Slope has a major effect on the rates of soil erosion, since, with increasing slope length and slope steepness, greater overland flow velocities occur and, therefore, more soil may be detached and transported (Alexakis et al. 2013). We calculated the combined LS factor by applying the following equation (Wischmeier and Smith 1978):

$$LS = \left( \frac{l}{72.6} \right)^m (65.41 \sin^2 \theta + 4.56 \sin \theta + 0.065) \quad (5)$$

where  $l$  is the cumulative slope length in meters,  $\theta$  is the downhill slope angle in % and  $m$  = slope contingent variable set to 0.5 if the slope angle is greater than 2.86°, 0.4 on slopes of 1.72° to 2.86°, 0.3 on slopes of 0.57° to 1.72°, and 0.2 on slopes less than 0.57° (Kumar et al. 2014).

### 3.3.5 Conservation Practice (P) Factor

The conservation practice, P, factor reflects the effects of practices, such as construction of terraces or contour strips, on the reduction of soil erosion. Practices of this kind can be found to a small extent across the island. However, historical information regarding its extent and

**Table 1** Soil parent material and estimated soil erodibility (K) factor for Thasos

Parent material	K factor
Alluvial deposits	0.15
Limestone	0.4
Schists	0.7
Tertiary deposits	0.15
Gneiss	0.3

intensity is not readily available and cannot be derived from medium-high satellite imagery. Therefore, in the present study, a P value equal to 1.0 was assigned throughout the entire study area.

## 4 Results and Discussion

The low differences among NDVI synthetic bands derived from TM, ETM+ and OLI sensors and their high linear correlation coefficients (Table 2), demonstrated that NDVI time series from these instruments can be used as complementary data for multi-temporal soil loss modelling. Following the absolute radiometric calibration based on the coefficients estimated upon PIFs (Table 2), using the Landsat-8 OLI image as a reference, the NDVI images were calculated. For the 1984 and 1991 image sets, a maximum NDVI composite generation procedure was followed in order to eliminate cloud- and shadow-covered areas. Alexandridis et al. (2013) demonstrated that there is a significant difference in the estimation of soil loss by erosion when variable time points are used for the C-factor estimation, due to the fact that vegetation conditions change rapidly during the year. However, seasonal crops are very limited in the specific area assessed in the present study. Since most of the LULC classes are permanent (e.g., pine trees, shrublands, olive trees etc.) and therefore the characteristics of their canopy does not change through the year, a single image acquisition within the same season for estimation of the NDVI is representative of the area's vegetation, as also noted by Alexakis et al. (2013).

The spatial extent of changes in soil erosion risk exhibited strong variations through the years of the analysis (1984–2013), as shown in Fig. 2. As expected, the lowest mean values of soil erosion were observed diachronically in the lowland areas (0–200 m elevation) along the coastline, while the highest erosion values were observed for the year 2000 in almost every elevation zone, ranging from 4.86 to 15.59 ton ha<sup>-1</sup>year<sup>-1</sup> (Table 3).

**Table 2** Multi-temporal regression slope (a) and Y-intercept (b), coefficient of determination (R<sup>2</sup>), and standard error (SE) of estimate values for the red and near-infrared (NIR) spectral band calibration of the 1984-TM5, 1991-TM4, 2000-ETM+ and 2007-TM5 to the 2013-OLI image

Sensor	Date	Band	Slope (a)	Y-intercept (b)	Coefficient of determination (R <sup>2</sup> )	Standard error (SE)
TM5	14/09/1984	Red	1.49	-0.025	0.93	0.03
		NIR	1.28	0.014	0.82	0.05
	30/09/1984	Red	1.44	-0.017	0.93	0.03
		NIR	1.16	0.047	0.79	0.05
TM4	08/07/1991	Red	1.13	-0.018	0.84	0.05
		NIR	1.06	0.029	0.83	0.04
	24/07/1991	Red	1.37	-0.026	0.87	0.04
		NIR	1.13	0.038	0.84	0.04
ETM+	24/08/2000	Red	1.36	-0.028	0.92	0.03
		NIR	1.34	-0.011	0.90	0.03
TM5	28/07/2007	Red	1.05	-0.046	0.93	0.03
		NIR	1.08	-0.022	0.85	0.03



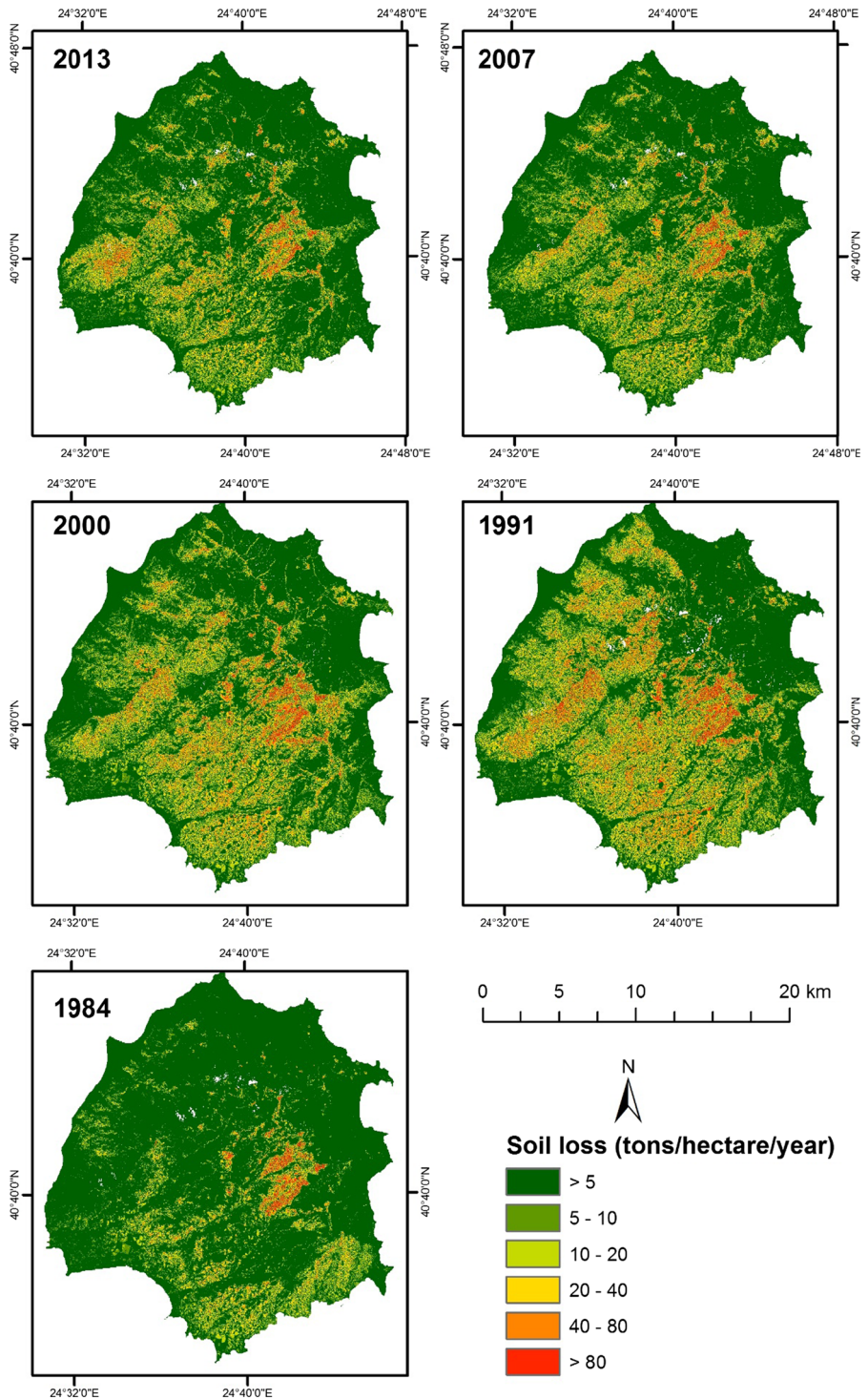


Fig. 2 Multi-temporal assessment of soil loss

**Table 3** Estimated mean soil erosion loss for the watersheds of Thassos island

Zone	Area (ha)	Estimated mean soil erosion loss (ton/ha/year)					Change (%) 1984–2013
		1984	1991	2000	2007	2013	
Aspect							
Flat	2429.36	0.00	0.01	0.01	0.00	0.00	39.05
North	8642.54	1.07	8.36	4.83	3.45	3.63	239.74
East	7489.58	4.80	12.70	10.34	7.76	7.31	52.23
South	10114.48	7.38	16.96	14.71	11.19	10.19	37.98
West	9265.19	3.37	11.06	8.30	6.29	5.81	72.76
Elevation							
0–200 m	14479.35	2.81	6.15	4.86	3.80	3.69	31.28
200–400 m	11859.83	4.06	13.59	10.02	7.45	6.81	67.90
400–800 m	9807.00	4.88	16.79	13.06	9.61	8.94	83.33
800–1203 m	1794.97	8.27	15.27	15.59	12.48	12.10	46.33

We observed a distinct pattern of erosion process for 1991, with higher values attained between 400 and 800 m of elevation, in contrast with the other years in the series, during which the most erosion-prone areas were located in the highest elevation zones (800–1200 m).

Assessment of the soil loss across different aspect classes indicated that the lowest values were attained in flat, mild areas of topography, as expected, while relatively low values were also attained in the northern slopes. The maximum values of soil loss occurred in south-facing slopes, ranging from 7.38 in 1984 to 16.96 ton ha<sup>-1</sup>year<sup>-1</sup> in 1991.

The soil erosion risk changes were the greatest (83.33 %) at elevation ranges between 400 and 800 m on Thassos, with high topographic potential for soil erosion. In lowlands along the coastline, there was only a subtle impact on soil, erosion, presumably resulting from the absence of any LUCC through time.

North-facing slopes exhibited the highest increase of soil loss through the 30-year period (108.42 %), and this was significantly higher than that observed for the east (52.23 %) and west slopes (72.96 %). However, the south-facing slopes remained the most vulnerable to degradation at all-time points.

The 10 watersheds of the island also exhibited strong variations in terms of soil loss through time. In nine of these, soil loss increased sharply during 1984–1991, while only one watershed presented a less sharp of approximately 38 % (Table 4). During the second period (1991–2000), soil loss decreased in two watersheds located in the east-northeast of Thassos (i.e., Panagia, Koinyron). In the subsequent time periods (2000–2007 and 2007–2013) mean soil loss decreased in all but the Kalliraxi watersheds of the island. Overall, during 1984–2013, soil loss was increased in all but Alykhs watershed, which showed a 38.41 % decrease.

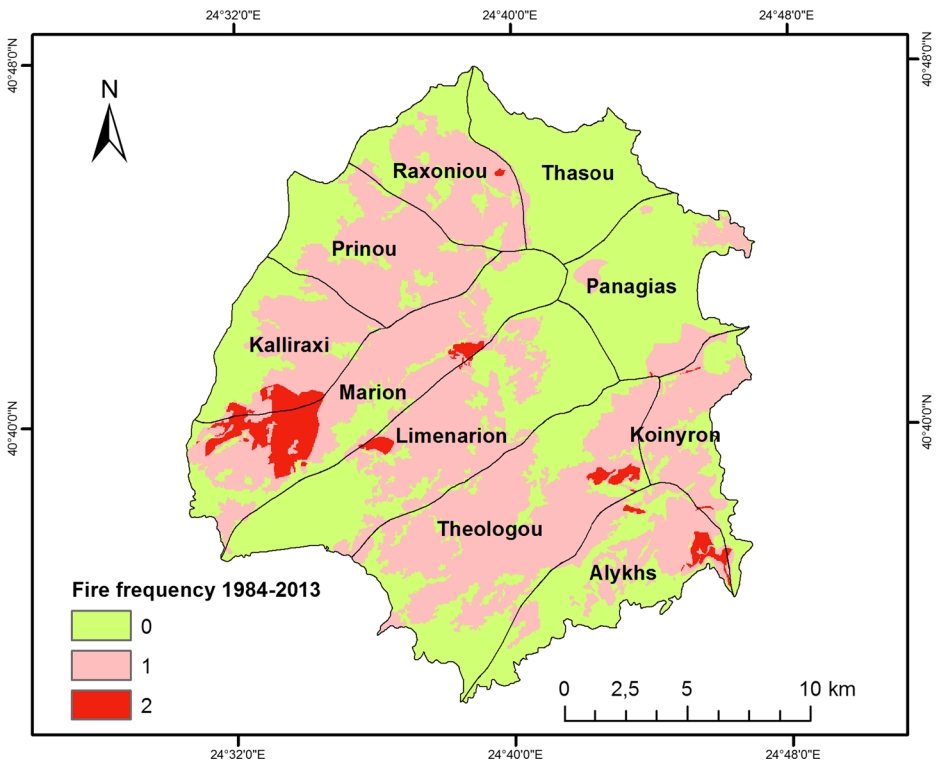
Fire history reconstruction over Thassos, quantifies the linkages between soil-erosion rates in mountainous and sub-mountainous regions of Mediterranean areas to fire-induced disturbances and the successional dynamics following regeneration of natural vegetation if left undisturbed. During the 1984–2013 period, fire activity as recorded in 10 different fire seasons, affected 20495 ha in total. The most devastating fires were detected in 1985, 1989 and 1984. The majority of the island (approx. 51 %) experienced fire spread and damage on at least one occasion, and up to 3 % of Thassos experienced a recurring fire during this period

**Table 4** Soil loss values for aspect and elevation ranges over Thasos

Watershed name	Area (ha)	Estimated mean soil erosion loss (ton/ha/year)					Change (%) 1984–2013
		1984	1991	2000	2007	2013	
Kalliraxi	2815	1.81	9.32	5.48	4.34	5.30	193.18
Prinou	3261	1.17	12.89	7.49	4.84	4.10	249.46
Raxoniou	2646	0.71	8.84	3.87	2.62	2.42	242.28
Thasou	2770	0.35	1.65	2.18	1.68	1.41	299.09
Marion	5083	2.32	14.90	9.85	8.16	9.82	323.93
Limenarion	5801	7.62	17.50	14.71	11.34	9.88	29.68
Theologou	6558	7.73	17.67	15.68	11.47	9.82	27.05
Panagias	3238	1.34	2.16	3.26	2.71	2.65	98.72
Koinyron	1832	0.98	4.29	5.25	3.32	2.80	186.11
Alykhs	2990	7.75	9.56	7.79	5.77	4.77	-38.41

(Fig. 3). In respect to individual watersheds, 16 % of the area of the of Marion watershed was burned twice throughout the 30 years studied, exhibiting the highest increase in soil erosion through time (Table 4).

The finding that soil loss remains increased in almost all the watersheds of the island despite the time elapsed from the devastating 1989 fire, confirms that wildfire can cause raised

**Fig. 3** Fire frequency during the 30 years of the analysis and watersheds of Thassos

sediment yields at the catchment scale for some considerable time after fire (Shakesby and Doerr 2006). While vegetation recovers relatively quickly in Mediterranean regions, leading to decline of soil erosion towards prefire conditions rates 3–4 years after burning, it is possible that changes in vegetation community structure may take place following repeated fires. Therefore, this alternation in vegetation structure and community, in the long run, may impact the erosional processes and the recovery of the entire system (Wittenberg and Inbar 2009). Small scale studies and plot measurements in Mt. Carmel, Israel (Wittenberg et al. 2014) and South-eastern Spain (del Pino JS and Ruiz-Gallardo 2014) also confirms the finding that soil loss amounts are commonly significantly higher on the south slope, steep gradients with north-facing slopes shown to be less prone to soil erosion than the rest.

While the fire-related abrupt LULCC represents the most dangerous changes, as the significant decrease of the protective function of forested areas may initiate strong erosion processes, other factors may have also influenced the soil loss and land degradation process in Thassos. Anthropogenic activities, such as mining and agricultural activities, may well have influenced the process and the pattern of erosion activity. Mouflis et al. (2008) monitored quarrying activity in Thassos between 1984 and 2000, and identified an almost 5-fold increase in the area used by quarries, which grew from 0.08 % of the landscape in 1984 to 180 ha, or 0.47 % of the island, in 2000, due to enlargement of existing quarries and the creation of new ones.

Another human activity shaping the landscape and increasing the risk of accelerated erosion is expected from ground-disturbing activities during fuels reduction treatments, such as construction of roads and firebreaks or salvage logging or thinning (Wondzell 2001). While it was not feasible to find historical records and maps documenting this hypothesis, visual interpretation of the multi-temporal satellite imagery used in the present study reveals that, between 1984 and 1991, where the large fires occurred, fire break and road density in the northern, intact forest part of the island considerably increased as a means of fire protection. We also visually interpreted the continuation of this trend in subsequent years.

On the basis of the multi-temporal assessment of soil loss process, land managers and risk planners can create spatially explicit erosion estimates to plan for watershed recovery treatments and erosion mitigation efforts. Despite the fact that the large area spatial assessment of soil loss from empirical models, is open to discussion due to the lack of measurement and validation data (Đukić and Radić 2014), the obtained relative assessment of soil loss conditions through time, between and within the catchments is deemed useful.

## 5 Conclusions

The scope of this study was the multi-temporal assessment of the soil loss process across Thassos, a fire-prone island in the eastern Mediterranean. Literature findings concerning measured rates of soil loss usually relate to small spatial and short temporal scales. Multitemporal landscape modelling can be used in order to understand the degradation processes and effects at larger scales.

We used imagery received from the TM, ETM+ and OLI instruments on board Landsat 4 and 5, Landsat 7 and Landsat-8 respectively. While previous studies addressing temporal and spatial explicit assessment of soil loss have relied on individual image classification, the results of the present study are based on the analysis of a multi-sensor NDVI image series that had been recorded using different spectral resolutions, and under variable atmospheric conditions

as a proxy for estimating the vegetation and biomass cover. Cross-calibration analysis of the NDVI images generated from the above sensors verified that they can be used as complementary data for soil-loss modeling.

Spatial temporal assessment of soil loss indicated significant differences along the four time intervals. With regard to the aspect, the most erosion-prone areas diachronically were the south-facing slopes. The highest altitudinal zone was most at soil-loss risk, but this elevation zone also has the smallest spatial extent compared to the others. A major increase for all the elevation and aspect zones, as well as for every watershed of the island, was observed during 1984–1991, when the island experienced some catastrophic fires. During 1984–2013, all but one of the watersheds of the island experienced a severe increase in soil erosion. The sharpest increase was recorded for a watershed burned during the last year of the analysis period. As the magnitude and effects of soil erosion processes are modified by a biophysical environment comprising soil, climate, terrain, and LULC, the fire regime of Thassos is a major driver of the change. Human activities, such as mining, and other ground disturbances, such as firebreaks and roads, also influence the distribution of the soil loss process.

The synergistic use of different generations of Landsat satellites facilitate the monitoring of the spatio-temporal change, pattern, and process of the earth's ecosystem. Knowledge of the spatial and temporal distribution of the erosion processes using landscape modeling, and its association with local environmental conditions, land utilization, and human activities, is crucial for effective land management decisions and mitigation of land degradation processes.

**Acknowledgments** Landsat TM, ETM+ and OLI data used were available at no-cost from the US Geological Survey. We would like to thank the Associate Editor and the 2 anonymous reviewers whose insightful comments helped to substantially improve this manuscript.

**Compliance with Ethical Standards** The manuscript has not been submitted to more than one journal for simultaneous consideration. The manuscript has not been published previously (partly or in full), unless the new work concerns an expansion of previous work. This study is not split up into several parts to increase the quantity of submissions and submitted to various journals or to one journal over time.

No data have been fabricated or manipulated (including images) to support the conclusions. No data, text, or theories by others are presented as if they were the author's own. Proper acknowledgements to other works is given, quotation marks are used for verbatim copying of material, and permissions are secured for material that is copyrighted.

Consent to submit has been received explicitly from all co-authors, as well as from the responsible authorities - tacitly or explicitly - at the institute/organization where the work has been carried out, before the work is submitted.

Authors whose names appear on the submission have contributed sufficiently to the scientific work and therefore share collective responsibility and accountability for the results. The authors do not disclosure of potential conflicts of interest and the research does not involves Human Participants and/or Animals

## References

- Alexakis DD, Hadjimitsis DG, Agapiou A (2013) Integrated use of remote sensing, GIS and precipitation data for the assessment of soil erosion rate in the catchment area of "Yialias" in Cyprus. *Atmos Res* 131:108–124
- Alexandridis TK, Sotiropoulou AM, Bilas G, Karapetsas N, Silleos NG (2013) The effects of seasonality in estimating the c-factor of soil erosion studies. *Land Degrad Dev*. In press
- Bajocco S, Salvati L, Ricotta C (2011) Land degradation versus fire: a spiral process? *Prog Phys Geogr* 35(1):3–18
- Butt M, Waqas A, Mahmood R (2010) The combined effect of vegetation and soil erosion in the water resource management. *Water Resour Manag* 24(13):3701–3714
- Cerdà A, Lavee H, Romero-Díaz A, Hooke J, Montanarella L (2010) Preface. *Land Degrad Dev* 21(2):71–74



- Chavez PS Jr (1996) Image-based atmospheric corrections - Revisited and improved. *Photogramm Eng Remote Sens* 62(9):1025–1036
- Chou WC (2010) Modelling watershed scale soil loss prediction and sediment yield estimation. *Water Resour Manag* 24(10):2075–2090
- Notario del Pino JS, Ruiz-Gallardo J-R (2014) Modelling post-fire soil erosion hazard using ordinal logistic regression: a case study in South-eastern Spain. *Geomorphology*: in press
- Đukić V, Radić Z (2014) GIS based estimation of sediment discharge and areas of soil erosion and deposition for the torrential Lukovska River catchment in Serbia. *Water Resour Manag* 28(13):4567–4581
- Flabouris K (2008) Study of rainfall factor R on the RUSLE law. PhD thesis. Faculty of Engineering, School of Civil Engineering, Aristotle University of Thessaloniki, Thessaloniki
- Gitas IZ, Devereux BJ (2006) The role of topographic correction in mapping recently burned Mediterranean forest areas from LANDSAT TM images. *Int J Remote Sens* 27(1):41–54
- Hijmans RJ, Cameron SE, Parra JL, Jones PG, Jarvis A (2005) Very high resolution interpolated climate surfaces for global land areas. *Int J Climatol* 25(15):1965–1978
- Jaiswal RK, Ghosh NC, Lohani AK, Thomas T (2015) Fuzzy AHP based multi criteria decision support for watershed prioritization. *Water Resour Manag* 29(12):4205–4227
- Kaltsas AM, Mamos AP, Tsatsarelis CA, Nanos GD, Kalburtji KL (2007) Energy budget in organic and conventional olive groves. *Agric Ecosyst Environ* 122(2):243–251
- Karydas C, Petriolis M, Manakos I (2013) Evaluating alternative methods of soil erodibility mapping in the Mediterranean Island of Crete. *Agriculture* 3(3):362–380
- Kouli M, Soupios P, Vallianatos F (2009) Soil erosion prediction using the Revised Universal Soil Loss Equation (RUSLE) in a GIS framework, Chania, Northwestern Crete. *Greece Environ Geol* 57(3):483–497
- Kumar S, Mishra A (2015) Critical erosion area identification based on hydrological response unit level for effective sedimentation control in a River Basin. *Water Resour Manag* 29(6):1749–1765
- Kumar A, Devi M, Deshmukh B (2014) Integrated remote sensing and geographic information system based RUSLE modelling for estimation of soil loss in western Himalaya. *India Water Resour Manag* 28(10):3307–3317
- Liu Y, Yang W, Yu Z, Lung I, Gharabaghi B (2015) Estimating sediment yield from upland and channel erosion at a watershed scale using SWAT. *Water Resour Manag* 29(5):1399–1412
- Lu D, Batistella M, Mausell P, Moran E (2007) Mapping and monitoring land degradation risks in the Western Brazilian Amazon using multitemporal Landsat TM/ETM+ images. *Land Degrad Dev* 18(1):41–54
- Mallinis G, Maris F, Kalinderis I, Koutsias N (2009) Assessment of post-fire soil erosion risk in fire-affected watersheds using remote sensing and GIS. *GISci and Remote Sens* 46(4):388–410
- Merritt WS, Letcher RA, Jakeman AJ (2003) A review of erosion and sediment transport models. *Environ Model Softw* 18(8–9):761–799
- Miller JD, Nyhan JW, Yool SR (2003) Modeling potential erosion due to the Cerro Grande Fire with a GIS-based implementation of the Revised Universal Soil Loss Equation. *Int J Wildland Fire* 12(1):85–100
- Morgan RPC (2005) Soil erosion and conservation. Oxford: Blackwell Pub, Malden
- Morschel J, Fox DM, Bruno JF (2004) Limiting sediment deposition on roadways: topographic controls on vulnerable roads and cost analysis of planting grass buffer strips. *Environ Sci Pol* 7(1):39–45
- Mouflis GD, Gitas IZ, Iliadou S, Mitri GH (2008) Assessment of the visual impact of marble quarry expansion (1984–2000) on the landscape of Thassos island, NE Greece. *Landscape Urban Plann* 86(1):92–102
- Nakos G (1979) General soil map of Greece
- Paolini L, Grings F, Sobrino JA, Jiménez Muñoz JC, Karszenbaum H (2006) Radiometric correction effects in Landsat multi-date/multi-sensor change detection studies. *Int J Remote Sens* 27(4):685–704
- Renard KG, Foster GR, Weesies GA, McCool DK, Yoder DC (1997) Predicting soil erosion by water: a guide to conservation planning with the Revised Universal Soil Loss Equation (RUSLE). *Agric Handbook* 703
- Schroeder TA, Cohen WB, Song C, Cauty MJ, Yang Z (2006) Radiometric correction of multi-temporal Landsat data for characterization of early successional forest patterns in western Oregon. *Remote Sens Environ* 103(1):16–26
- Shakesby RA, Doerr SH (2006) Wildfire as a hydrological and geomorphological agent. *Earth-Sci Rev* 74(3–4):269–307
- Simms É, Ward H (2013) Multisensor NDVI-based monitoring of the tundra-taiga interface (Mealy Mountains, Labrador, Canada). *Remote Sens* 5(3):1066–1090
- Siyan W, Jingshi L, Cunjian Y (2007) Temporal change in the landscape erosion pattern in the Yellow River Basin, China. *Int J Geogr Inf Sci* 21(10):1077–1092
- Steven MD, Malthus TJ, Baret F, Xu H, Chopping MJ (2003) Intercalibration of vegetation indices from different sensor systems. *Remote Sens Environ* 88(4):412–422
- Tamene L, Le Q, Vlek PG (2014) A landscape planning and management tool for land and water resources management: an example application in northern Ethiopia. *Water Resour Manag* 28(2):407–424

- Tucker CJ (1979) Red and photographic infrared linear combinations for monitoring vegetation. *Remote Sens Environ* 8(2):127–150
- Van der Knijff JM, Jones RJA, Montanarella L (1999) Soil erosion risk assessment in Italy. In Luxembourg, p 52
- Vrieling A (2006) Satellite remote sensing for water erosion assessment: a review. *Catena* 65(1):2–18
- Wang L, Huang J, Du Y, Hu Y, Han P (2013) Dynamic assessment of soil erosion risk using landsat TM and HJ satellite data in Danjiangkou Reservoir Area, China. *Remote Sens* 5(8):3826–3848
- Wischmeier WH, Smith DD (1978) Predicting rainfall erosion losses. In: *Agricultural handbook*. Wischmeier WH, Smith DD. 1978. Predicting rainfall erosion losses, agricultural handbook 537. USDA Scientific and Educational Administration: Washington
- Wittenberg L, Inbar M (2009) The role of fire disturbance on runoff and erosion processes - a long-term approach, Mt. Carmel case study, Israel. *Geogr Res* 47(1):46–56
- Wittenberg L, Malkinson D, Barzilai R (2014) The differential response of surface runoff and sediment loss to wildfire events. *Catena* 121:241–247
- Wondzell SM (2001) The influence of Forest Health and Protection treatments on erosion and stream sedimentation in forested watersheds of eastern Oregon and Washington. *Northwest Sci* 75(SPEC. ISS):128–140
- Zhao H, Chen X, Zhang J, Yin Z (2012) Land-use/-cover change spatial patterns and their impacts on sediment charge in the Longchuan River catchment, south-western China. *Int J Remote Sens* 33(14):4527–4552